HEPSY-94-5
Fermilab Library
0 1160 0052193 4

HEPSY 94-5
Sept. 1994

FERMILAB
SEP 199

FUNDAMENTAL CONSTANTS FROM b AND c DECAY

Sheldon Stone

Physics Department, Syracuse University

Syracuse, N.Y. 13244-1130, U. S. A.

NAME | ID No | M.S.
RETURN TO FERMILAB LIBRARY

Invited talk presented at "Particles, Strings and Cosmology" (PASCOS) meeting Syracuse, N.Y., May 1994, and portions of at TSAI, Boulder, Colorado, June, 1994, and DPF meeting, Albuquerque, N.M. August 1994

FUNDAMENTAL CONSTANTS FROM b AND c DECAY

SHELDON STONE
Physics Department, Syracuse University
Syracuse, N.Y. 13244, U. S. A.

ABSTRACT

Best estimates of the CKM matrix elements V_{cb} and V_{ub}, of 0.038±0.003 and 0.0030±0.0008, are extracted from data on semileptonic b decays. This information is combined with results on $B-\bar{B}$ mixing and CP violation in K_L^0 decay in order to determine constraints on standard model parameters. Expectations of CP violating angles in the B system and B_s mixing are given.

1. Introduction - some fundamental items

In the "Standard Model,"[2] the fundamental entities are pointlike spin-1/2 objects. The left-handed quarks are assigned to fractionally charged doublets, similar to the leptons which, however, have integral charge. Both quarks and leptons appear with a three-fold recurrence, as shown in Fig. 1. Heavy quarks, are considered to be the last two of these. (Left-handed objects have the helicity quantitized opposite to their direction of motion.)

$$\begin{pmatrix} u \\ d \end{pmatrix} \begin{pmatrix} c \\ s \end{pmatrix} \begin{pmatrix} t \\ b \end{pmatrix} \begin{matrix} Q = +2/3 \\ Q = -1/3 \end{matrix}$$

$$\begin{pmatrix} \nu_e \\ e \end{pmatrix} \begin{pmatrix} \nu_\mu \\ \mu \end{pmatrix} \begin{pmatrix} \nu_\tau \\ \tau \end{pmatrix} \begin{matrix} Q = 0 \\ Q = -1 \end{matrix}$$

Fig. 1. The three families of quarks and lepton doublets

The masses of quarks are somewhat ill defined, and hard to measure. This is due to the fact that quarks possess color and don't exist freely in nature. I won't discuss this topic, nor will I discuss the couplings α, G_F, α_s, $sin\theta_W$, which are related to forces. What I will discuss are the quark couplings. They may be understood as resulting from the mixture of the charge = -1/3 quarks. The mass eigenstates (unprimed) are related to the weak eigenstates states (primed) via the Cabibbo-Kobayashi-Maskawa matrix shown in Fig. 2.

$$\begin{pmatrix} d' \\ s' \\ b' \end{pmatrix} = \begin{pmatrix} V_{ud} & V_{us} & V_{ub} \\ V_{cd} & V_{cs} & V_{cb} \\ V_{td} & V_{ts} & V_{tb} \end{pmatrix} \begin{pmatrix} d \\ s \\ b \end{pmatrix}$$

Fig. 2. The CKM matrix relationship between the mass eigenstates (unprimed) and the weak eigenstates (primed).

The 9 complex matrix elements are fundamental constants that need to be determined from experiment. They can be expressed in terms of 4 parameters. A useful first order expansion, due to Wolfenstein,[1] is shown in Fig. 3.

$$V_{ij} = \begin{pmatrix} 1-\lambda^2/2 & \lambda & A\lambda^3(\rho - i\eta) \\ -\lambda & 1-\lambda^2/2 & A\lambda^2 \\ A\lambda^3(1-\rho-i\eta) & -A\lambda^2 & 1 \end{pmatrix}$$

Fig. 3. The Wolfenstein parameterization of the CKM matrix

The parameters λ and A are determined from charged current decays. The simplest charged current decay is that of the muon. A diagram of the decay is shown in Fig. 4. The decay rate can be expressed as

$$\Gamma_\mu = \frac{G_F^2 m_\mu^5}{192\pi^3} \times (\text{radiative correction}) \times (\text{phase space}). \tag{1}$$

This process is used, in fact, to determine G_F.

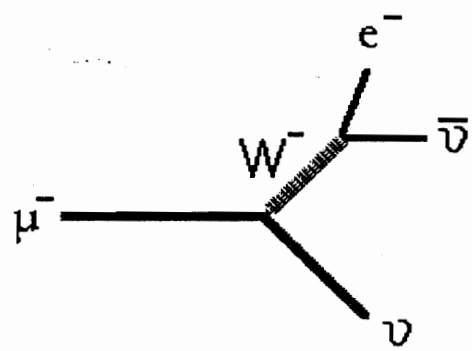

Fig. 4. Feynman diagram of muon decay.

An example of a charged current process for quarks is strange quark decay; a sample diagram is shown in Fig. 5. By measuring the decay rate of kaon and hyperon semileptonic decays, and after applying suitable corrections, a value of

$$\lambda = V_{us} = 0.2205 \pm 0.0018 \tag{2}$$

is found.[3] Measurements of V_{cd} and V_{cs} agree with this value. Similarly, A is determined from $b \to c\ell\nu$ decays. Constraints on ρ and η are found from other measurements.

The fact that the CKM matrix is complex allows CP violation for 3 or more generations, as first shown by Kobayashi and Maskawa. C is defined as a quantum mechanical operator that takes particle to antiparticle, and P is an operator that switches left to right. Examples of CP violation have been found in the K^0 system.[4] Consider the K^0 to be the superposition of two weak eigenstates a short lived kaon, K_s, with lifetime 9×10^{-11} sec., and a long lived kaon with lifetime 5×10^{-8} sec., then

$$\left|K^0\right\rangle = \frac{1}{\sqrt{2}}\left(|K_s\rangle + |K_L\rangle\right). \tag{3}$$

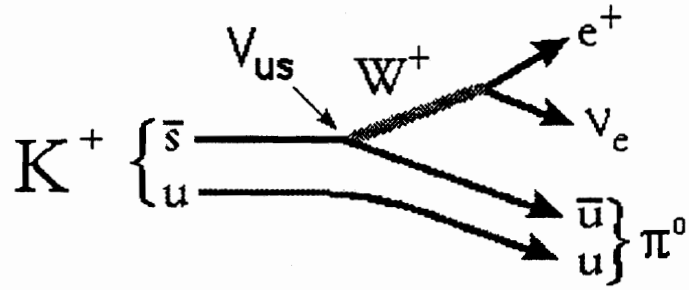

Fig. 5. Quark level diagram of K^+ decay. The relevant CKM couplings are indicated.

If we start out with a K^0 beam, after the K_s decay away, we have only K_L left. Then it is observed that the K_L decays in two ways: $K_L \to e^+\nu_e\pi^-$ and $K_L \to e^-\bar{\nu}_e\pi^+$. Recall that the initial K^0 was formed from an $\bar{s}$ d pair. The $\bar{s}$ must decay into a e^+ as shown in Fig. 5.

Thus in the K_L decay there is evidence that both K^0 and $\bar{K}^0$ are present. This phenomena where a K^0 can transform into a $\bar{K}^0$ and vice-versa is called mixing, and can be described by the "box" diagram shown in Fig. 6.

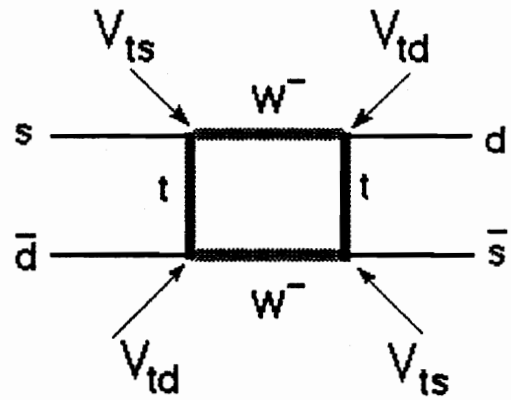

Fig. 6. Quark level diagram mixing in the K^0 system. The relevant CKM couplings are indicated.

An example of CP violation is

$$\frac{rate(K_L \to e^+\nu_e\pi^-) - rate(K_L \to e^-\bar{\nu}_e\pi^+)}{rate(K_L \to e^+\nu_e\pi^-) + rate(K_L \to e^-\bar{\nu}_e\pi^+)} = 3 \times 10^{-3}. \tag{4}$$

To see why this rate asymmetry is an example of CP violation, look at Fig. 7. The C operator changes particle to antiparticle, while the P operator reverses the direction of momentum but doesn't change spin. Thus the final state containing a right-handed positron is transformed in the final state containing a left-handed electron by the CP operation. If CP were conserved the rate asymmetry would be zero.

In the Standard Model, CP violation results from the interference between "tree" decay diagram and the "box" decay mixing diagram. *If we could find CP violation*

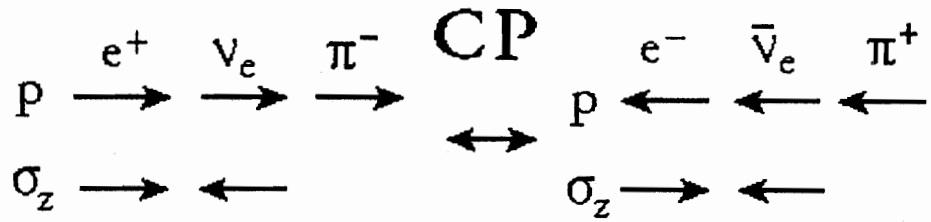

Fig. 7. Effect on momentum and spin vectors of the CP operation on the final state $\pi e \nu$.

in the B system we could see if the standard model works or perhaps go beyond the model. Speculation has it that CP violation is responsible for the baryon-antibaryon asymmetry in our section of the Universe. *If so, understanding the mechanism of CP violation is critical in our conjectures of why we may exist.*

2. CKM Elements from B decays

2.1. V_{cb}

2.1.1. Introduction

The charged current semileptonic B decay diagram, used for the study of V_{ub} and V_{cb}, is shown in Fig. 8. Either inclusive or exclusive decays can be used to extract the CKM elements. It is informative to consider the fraction of semileptonic decays of heavy mesons to the lowest lying exclusive finals states, those with a pseudoscalar or vector meson in the final state, see Table 1.

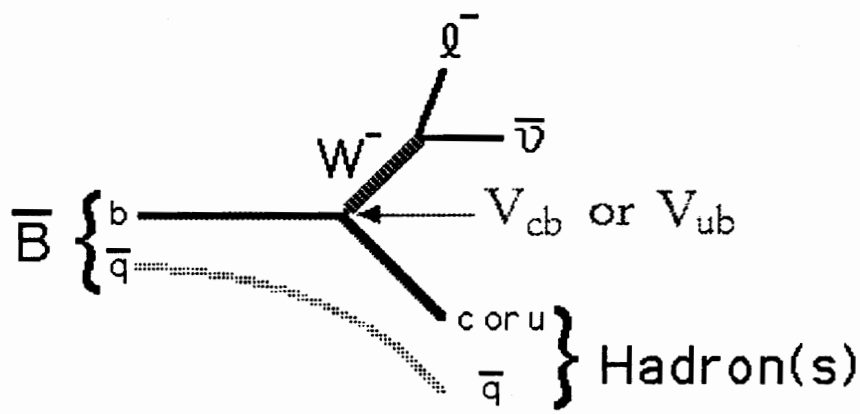

Fig. 8. Diagram discribing semileptonic B decays.

Whereas strange or charm decays must use exclusive final states to ascertain the value of λ, bottom decays can use both exclusive and inclusive decays to determine V_{cb} and possibly V_{ub}. I will discuss three different ways of determining V_{cb}, all with comparable accuracy.

Table 1. Fraction of $Q \to q\ell\nu$ to lowest lying states

quark	percentage	process
s	100%	$K \to \pi\ell\nu$
c	>90%	$D \to (K + K^*)\ell\nu$
	?	$D \to (\pi + \rho)\ell\nu$
b	≈66%	$B \to (D + D^*)\ell\nu$
	?	$B \to (\pi + \rho)\ell\nu$
t	0%	t does not form hadrons

2.1.2. Exclusive Decays

For decays of a pseudoscalar B to a lighter pseudoscalar meson, m, plus a lepton and neutrino, the decay amplitude can be written as a product of two currents, a lepton current, L^μ, and a hadron current, H_μ,

$$A(\bar{B} \to me^-\bar{\nu}) = \frac{G_F}{\sqrt{2}} V_{ij} L^\mu H_\mu, \text{ where} \tag{5}$$

$$L^\mu = \bar{u}_e \gamma^\mu (1 - \gamma_5) v_\nu, \text{ and} \tag{6}$$

$$H_\mu = \langle m | J^\mu_{had}(0) \left| \bar{B} \right\rangle = f_+(q^2)(p + P)_m + f_-(q^2)(p - P)_m, \tag{7}$$

where q^2 is the 4-momentum transfer between the B and the m. Since the term multiplying $f_-(q^2)$ contains the square of the lepton mass, the resulting semileptonic width doesn't depend on this form factor for electronic or muonic decays. The width is:

$$\frac{d\Gamma(B \to m\ell\bar{\nu})}{dq^2} = \frac{|V_{ij}|^2 K^3}{24\pi^3} |f_+(q^2)|^2, \tag{8}$$

where K is the momentum of the m in the B rest frame given by:

$$K = \frac{1}{2m_B} \left[\left(m_B^2 + m_m^2 - q^2 \right)^2 - 4m_B^2 m_m^2 \right]^{\frac{1}{2}}, \tag{9}$$

where, m_B and m_m are, respectively, the B and m masses. We must get $f_+(q^2)$ from theory. (In principle, the shape can be measured and only the normalization must be obtained theoretically.) Then V_{cb} can be determined from measurements of the branching ratio and the lifetime, τ_b, since

$$\Gamma(B \to m\ell\bar{\nu}) = \frac{1}{24\pi^3} |V_{cb}|^2 \int K^3 |f_+(q^2)|^2 dq^2, \text{ and} \tag{10}$$

$$\Gamma(B \to m\ell\bar{\nu}) = \mathcal{B}(B \to m\ell\bar{\nu}) \cdot \Gamma_{tot} = \frac{\mathcal{B}(B \to m\ell\bar{\nu})}{\tau_b} \tag{11}$$

The particular realization of pseudoscalar to pseudoscalar decay is $B \to D\ell\bar{\nu}$. However, the data are imprecise. It is much easier to analyze $D^*\ell\bar{\nu}$ final states, because use of the $D^* - D$ mass difference causes a large reduction of background in D^* final

states, and because the $D^*\ell\bar{\nu}$ final state has a much larger branching ratio. In this case there are 3 form factors, due to the vector nature of the D^*. Explict formulas analogous to equations (7-11) are given in ref. [5].

2.1.3. Measurements of $\mathcal{B}(B \to D^*\ell\bar{\nu})$

After selecting candidate D^* and candidate leptons, the missing mass squared is used to find the signal. The missing mass squared is calculated as:

$$MM^2 = (E_B - (E_{D*} + E_\ell))^2 - (\vec{p}_B - (\vec{p}_{D*} + \vec{p}_\ell))^2. \tag{12}$$

The B meson energy, E_B, is set equal to the beam energy, E_{beam}, and the B momentum, p_B, which is 325 MeV/c, is approximated as zero because the direction is unknown. Then

$$MM^2 = (E_{beam} - (E_{D*} + E_\ell))^2 - (\vec{p}_{D*} + \vec{p}_\ell)^2 \tag{13}$$

Signal events will have a missing mass consistent with zero. The approximation of setting p_B=0 causes the MM^2 distribution to be widened significantly; this is much larger than any widening caused by detector mismeasurements.

This technique has been used for isolating exclusive decays into both $D^{*+}\ell^-\bar{\nu}_\ell$ and $D^{*0}\ell^-\bar{\nu}_\ell$. Let us consider first the case of the D^{*+}. Monte Carlo simulation of the MM^2 for this reaction and from possible background reactions including $B \to D^{**}\ell^-\bar{\nu}_\ell$ are shown in Fig. 9 . Here it matters little if the D^{**} is a resonance or just a low mass non-resonant $D^*\pi$ system. Data from ARGUS, which pioneered this technique, is shown in Fig. 10. The branching ratio measurements are given in Table 2.

Table 2. $\mathcal{B}(B \to D^*\ell^-\bar{\nu})\left(\frac{0.5}{f_i}\right)$ (%)

Mode	CLEO[6]	ARGUS[7,8]	CLEO II[9]	Average
$D^{*+}\ell^-\bar{\nu}$	4.1±0.5±0.7	4.7±0.6±0.6	4.49±0.32±0.39	4.46±0.39
$D^{*0}\ell^-\bar{\nu}$		6.8±1.6±1.5	5.13±0.54±0.64	5.3±0.8

To extract $|V_{cb}|$, I use the average branching ratio for $\mathcal{B}(\overline{B}^0 \to D^{*+}\ell^-\bar{\nu})$ and $\mathcal{B}(B^- \to D^{*0}\ell^-\bar{\nu})$ from CLEO II only, since this is the only experiment which has measured both of these rates accurately. In this average branching ratio the poorly known fractions of neutral, f_0 and charged, f_-, $B's$ from $\Upsilon(4S)$ decay cancel and do not add to the uncertainty. Explicitly,

$$< B >= f_0\mathcal{B}(\overline{B}^0 \to D^{*+}\ell^-\bar{\nu})\left(\frac{0.5}{f_0}\right) + f_-\mathcal{B}(B^- \to D^{*0}\ell^-\bar{\nu})\left(\frac{0.5}{f_-}\right) = (4.72 \pm 0.52)\% \tag{14}$$

These branching ratios can be used directly to find V_{cb} when combined with lifetime measurements from other experiments. I use 1.53±0.09 ps, 1.68±0.12 ps, and 1.58±0.07 ps, for the lifetimes of $\overline{B}^0$, B^- and their average, respectively.[10] Using these values, the experimental value of the width for $\Gamma(B \to D^*\ell^-\bar{\nu})$ is $(29.9 \pm 2.3 \pm 2.7)$ ns^{-1}. The resulting values for V_{cb} are given in Table 3, along with the predicted values for the width.

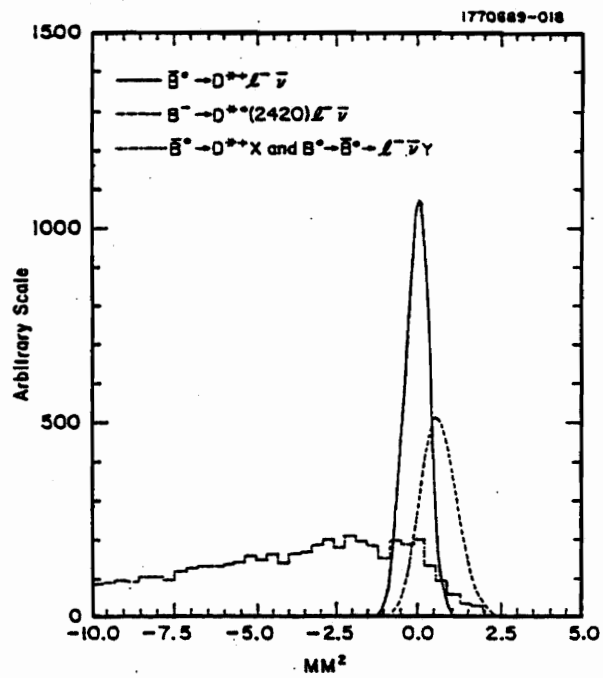

Fig. 9. Missing mass squared distributions for signal and background processes.

Table 3. Values of $|V_{cb}|$ from $\Gamma(B \to D^*\ell^-\bar{\nu})$

Model	$\Gamma(B \to D^*\ell^-\bar{\nu})$ps	$\lvert V_{cb}\rvert$
ISGW[11]	$25.2\lvert V_{cb}\rvert^2$	0.0344±0.0021
KS[12]	$25.7\lvert V_{cb}\rvert^2$	0.0341±0.0020
WBS[13]	$21.9\lvert V_{cb}\rvert^2$	0.0369±0.0022
Jaus[14]	$21.7\lvert V_{cb}\rvert^2$	0.0371±0.0022

I take an average value, in the center of the model predictions, and include an error due to the range of the model predictions. This gives a value

$$|V_{cb}| = 0.0356 \pm 0.0022 \pm 0.0015. \tag{15}$$

The first error is formed from the errors on the branching ratio (±3.0%) and the lifetime (±2.3%) , while the second error arises from the model dependence (±4.2%).

2.1.4. V_{cb} using the "Universal" form factor

One theory based on QCD, called Heavy Quark Effective Theory (HQET),[15] assumes very heavy quarks. Then the spin degrees of freedom decouple, and there is only one form factor function $\xi(y)$ which is a function of the Lorentz invariant 4-velocity transfer y

$$y = \frac{M_B^2 + M_{D^*}^2 - q^2}{2M_B M_D^*}. \tag{16}$$

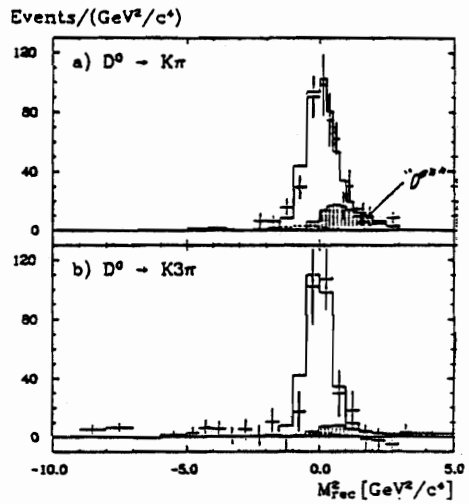

Fig. 10. Missing mass squared data from ARGUS for the $D^* + \ell^- \bar{\nu}$ final state, for two different D^0 decay modes

The point y equals 1 corresponds to the situation where the B decays to a D^* which is at rest in the B frame. At this point the "universal" form factor function $\xi(y)$ has the value $\xi(1) = 1$ in lowest order. There are, however, corrections even at $y = 1$. These are due to hard gluons, which cause a first order correction, and the finite values of the b and c quark masses, which enter only in second order. Neubert estimates the correction factor as 0.97 ± 0.04 for $\xi(1)$.[16] This value has been challanged by a QCD sum rule calculation of Shifman et al.;[17] they set an upper limit of < 0.94 and give an "educated guess" of 0.89 ± 0.03.

In order to find the experimental value of the cross section at y of one, the data need to be fit to an "unknown" functional form. The curvature is expected to be positive, since there is a pole as y approaches 1, outside of the physical region, and $\xi(y) \to 0$ as y increases.

CLEO[9] assumes the form

$$\xi(y) = \xi(1) - \rho^2(y-1) + b(y-1)^2, \tag{17}$$

which represents a second order expansion in the vicinity of y of one. The CLEO data plotted as function of y are shown in Fig. 11. The resulting values are shown in Table 4. The b parameter is found to be consistent with zero and the second row reflects the result of the fit with b constrained to be zero. The first error is due the statistical uncertainty, including the uncertainty due to the background, while the second gives the systematic uncertainty.

CLEO uses the latter value to extract a value of $|V_{cb}|\xi(1)$, although it would be more conservative to use the unconstrained b parameter fit. Another way of seeing what the error is, due to various shapes of $\xi(y)$, is to fit the data points to different forms that have been predicted theoretically. I have done this using the CLEO data points. The fits are shown in Fig. 12 and the results given shown in Table 5.

The values extracted for V_{cb} using either the Neubert or Shifman estimates for the QCD corrections are shown in Table 6. The first two entries, for the linear and quadratic fits give the CLEO values from Table 4, while the last three entries are

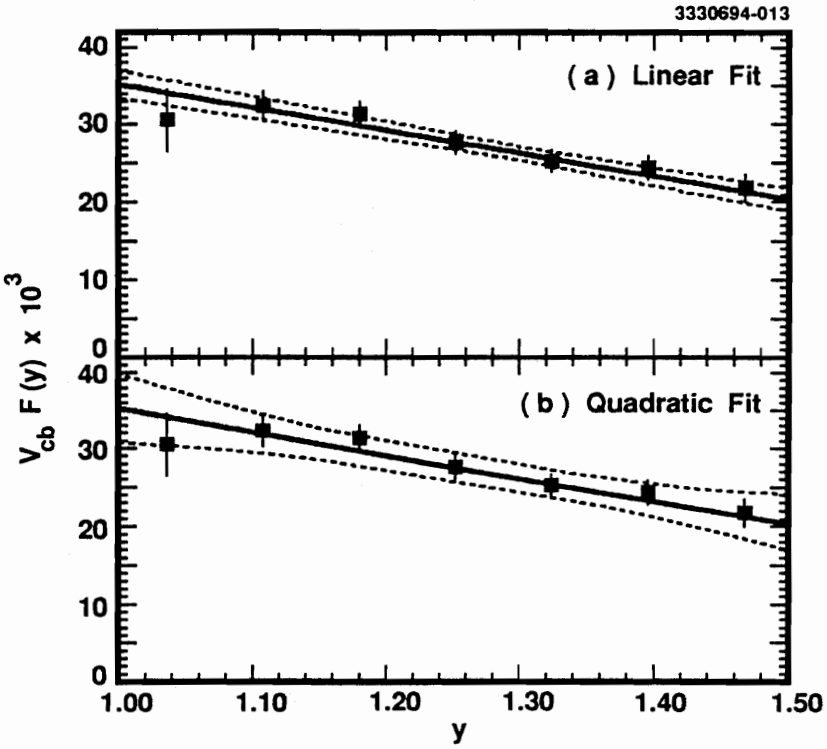

Fig. 11. Linear and quadratic fits to the CLEO data. $F(y)$ is equivalent to $\xi(y)$ as used in this paper.

Table 4. Values for $|V_{cb}|\xi(1)$ from CLEO data

$\|V_{cb}\|\xi(1)$	ρ^2	b
0.0353± 0.0032±0.0030	0.92±0.64±0.40	0.15±1.24±0.90
0.0351± 0.0019±0.0019	0.84±0.13±0.08	0

derived from Table 5. The quoted errors are the quadrature of the errors given in the above mentioned tables.

Using the average of the values derived using the Neubert and Shifman values for $\xi(1)$,[18] and the exponential fit, I derive a value of

$$|V_{cb}| = 0.0387 \pm 0.0030 \pm 0.0020, \tag{18}$$

where the last error results from the spread in functional forms and theoretical values for $\xi(1)$.

2.1.5. V_{cb} from Inclusive Decays

What is actually measured here is the semileptonic branching ratio $\mathcal{B}(B \to Xe^-\bar{\nu})$. While this has traditionally been done by measuring the inclusive lepton momemtum spectrum using only single lepton data, recently dilepton data have been used. The inclusive lepton spectrum from the latest CLEO II data is shown in Fig. 13. Both

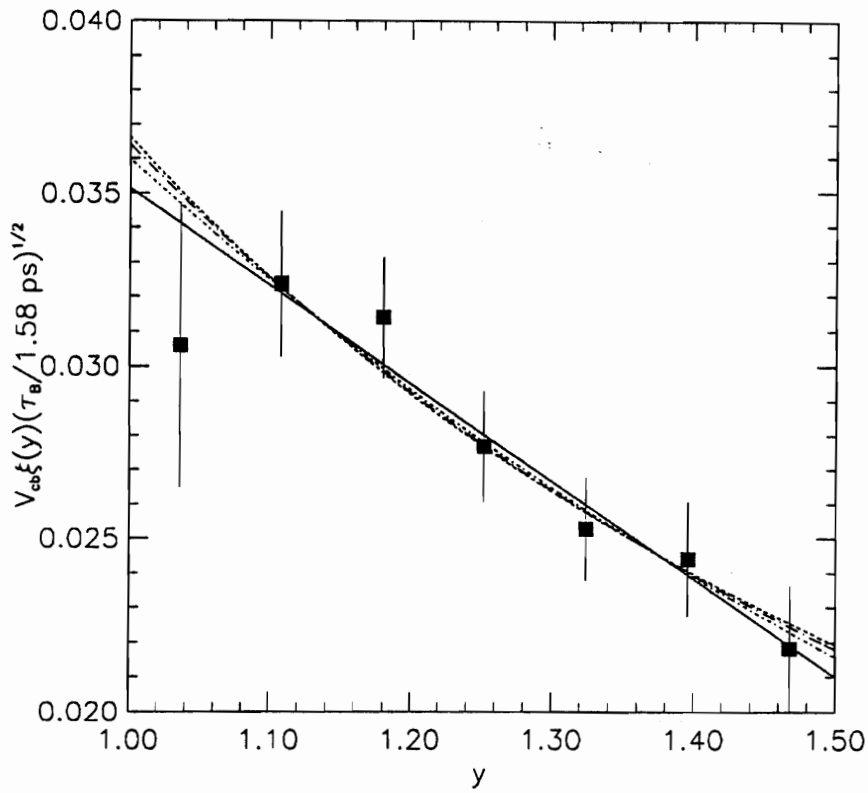

Fig. 12. Fits to the CLEO data with the functions listed in Table 5.

electrons and muons are shown. Leptons which arise from the continuum have been statistically subtracted using the below resonance sample. The peak at low momentum is due to the decay chain $\bar{B} \to DX$, $D \to Y\ell^+\nu$. The data are fit to two shapes whose normalizations are allowed to float. The first shape is taken from models of B decay while the second comes from the measured shape of leptons from D mesons produced nearly at rest at the ψ'', which is then smeared using the measured momentum distribution of $D's$ produced in B decay. CLEO finds $\mathcal{B}_{sl}$ of 10.5±0.2% and 11.1±0.3% in the ACM[19] and ISGW* models, respectively.[20]

Next, I discuss how to use dilepton events to eliminate the secondary leptons at low momentum. Consider the sign of the lepton charges for the four leptons in the following decay sequence: $\Upsilon(4S) \to B^-B^+$; $B^- \to D\ell_1^-\bar{\nu}$, $B^+ \to \bar{D}\ell_3^+\nu$; $D \to Y\ell_2^+\nu$, $\bar{D} \to Y'\ell_4^-\bar{\nu}$. If a high momentum negative lepton (ℓ_1^-) is found, then if the second lepton is also negative it must come from the cascade decay of the B^+ (i.e. it must be ℓ_4^-). On the other hand the second lepton being positive shows that it must be either the primary lepton from the opposite B^+, (ℓ_3^+), or the cascade from the same B^-, (ℓ_2^+). However the cascades from the same B^- can be greatly reduced by insisting that the cosine of the opening angle between the two leptons be greater than zero as they tend to be aligned. The same arguments are applicable to $\Upsilon(4S) \to B^0\overline{B}^0$, except that an additional correction must be made to account for $B\bar{B}$ mixing.

The CLEO II data are shown in Fig. 14. The data fit nicely to either the ACM or ISGW model. They find that the semileptonic branching ratio, $\mathcal{B}_{sl}$, equals $(10.36 \pm 0.17 \pm 0.40)\%$ with a negligible dependence on the model.[22] This result confirms that

Table 5. Values for $|V_{cb}|\xi(1)$ from fits to different shapes

$\xi(y)$	name	ρ	$V_{cb}\xi(1)$
$1-\rho^2(y-1)$	linear	0.90±0.07	0.0351±0.0018±0.0018
$\frac{2}{y+1}exp\left[-(2\rho^2-1)\frac{y-1}{y+1}\right]$	NR exp	0.90±0.12	0.0366±0.0024±0.0018
$\left(\frac{2}{y+1}\right)^{2\rho^2}$	pole	1.07±0.11	0.0364±0.0023±0.0018
$exp\left[-\rho^2(y-1)\right]$	exp	1.01±0.10	0.0360±0.0022±0.0018

Table 6. Values for $|V_{cb}|$

$\xi(y)$	name	V_{cb} (Neubert)	V_{cb} (Shifman)
$1-\rho^2(y-1)+b(y-1)^2$	quadratic	0.0364±0.0045	0.0397±0.0049
$1-\rho^2(y-1)$	linear	0.0362±0.0030	0.0395±0.0033
$\frac{2}{y+1}exp\left[-(2\rho^2-1)\frac{y-1}{y+1}\right]$	NR exp	0.0377±0.0031	0.0411±0.0034
$\left(\frac{2}{y+1}\right)^{2\rho^2}$	pole	0.0375±0.0030	0.0409±0.0033
$exp\left[-\rho^2(y-1)\right]$	exp	0.0371±0.0029	0.0404±0.0032

the B model shapes are appropriate down to lepton momenta of 0.6 GeV/c. ARGUS[21] did the first analyis using this technique and found $\mathcal{B}_{sl} = (9.6 \pm 0.5 \pm 0.4)\%$.

Consider $\Gamma_{sl} \equiv \Gamma(B \to Xe^-\bar{\nu})$ in the simplest parton model:

$$\Gamma_{sl} = \frac{G_F^2 m_b^5}{192\pi^3}\left(p_c|V_{cb}|^2 + p_u|V_{ub}|^2\right)\eta_{QCD}, \tag{19}$$

where the p's are phase space factors, and the QCD correction, $\eta_{QCD} = 1 - 2\alpha_s/39$. Since $|V_{ub}| << |V_{cb}|$, we ignore the 2nd term. To use the semileptonic width to extract $|V_{cb}|$ using this expression requires a knowledge of m_b^5, which is poorly understood. A way around this dilemma was found by Altarelli et al.[19] They make two important corrections to the simple parton model. First they treat the spectator quark in the B meson as a quasi-free particle with a Gaussian spectrum of Fermi-momentum, p:

$$f(p) = \frac{4p^2}{\sqrt{\pi}p_f^3}\exp(-p^2/p_f^2). \tag{20}$$

The average value, p_f, is a free parameter in the model. Secondly, they include the effects of gluon radiation from the quarks, which lowers the spectrum at high lepton momentum. The semileptonic width is given explicitly as:

$$\frac{d\Gamma(B \to DX\ell^-\overline{\nu}_\ell)}{dx} = \frac{m_b^5 G_F^2 V_{cb}^2}{96\pi^3}\cdot\left[\Phi(x,\epsilon) - G(x,\epsilon)\right], \tag{21}$$

where $x = 2E_\ell/m_b$, E_ℓ being the lepton energy, $\epsilon = m_c/m_b$, $G(x,\epsilon)$ is a complicated gluon radiation function and

$$\Phi(x,\epsilon) = \frac{x^2(1-\epsilon^2-x)^2}{(1-x)^3}\left[(1-x)(3-2x) + (3-x)\epsilon^2\right]. \tag{22}$$

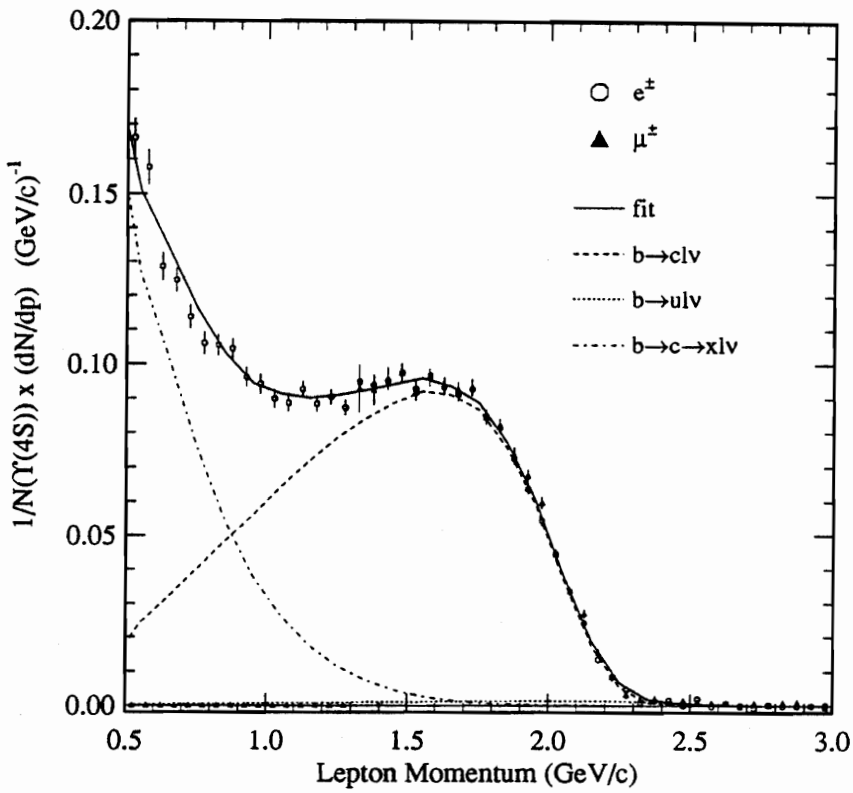

Fig. 13. Fit to the CLEO inclusive lepton spectrum with the ACM model.

Each value of the Fermi-momentum, p, leads to a different value of m_b and hence a different distribution for $\frac{d\Gamma}{dx}$ which must be convoluted with Eq. (21) to find the total theoretical lepton momentum spectrum. The relationship between m_b and p is just given by kinematics

$$m_b^2 = m_B^2 + m_{sp}^2 - 2m_B\sqrt{(p^2 + m_{sp}^2)}. \tag{23}$$

Here m_B is the known value of the B meson mass of 5.280 GeV and m_{sp} is the spectator quark mass. A fit to the shape of the lepton energy spectrum then is needed to determine the free parameters p_f, ϵ and m_{sp}. In turns out that one can fix m_{sp} and any latent dependence is absorbed by the other two. So a fit to the data will determine $\mathcal{B}_{sl}$, p_f and ϵ. In this way Altarelli et al. remove the explicit dependence of the m_b^5 term in the total decay rate.

We can also use the ISGW model because it includes final states beyond D and D^*. CLEO also lets the "extra" component float it the fit. This model is named ISGW*. The resulting values are given in Table 7.

The representative value of $|V_{cb}|$ found from this analysis alone is $0.0395 \pm 0.0010 \pm 0.0040$.

2.1.6. Average of all three methods

The values of V_{cb} derived using all three methods are shown in Fig. 15. Consistent results are found. An average value is derived using all three results, but adding the

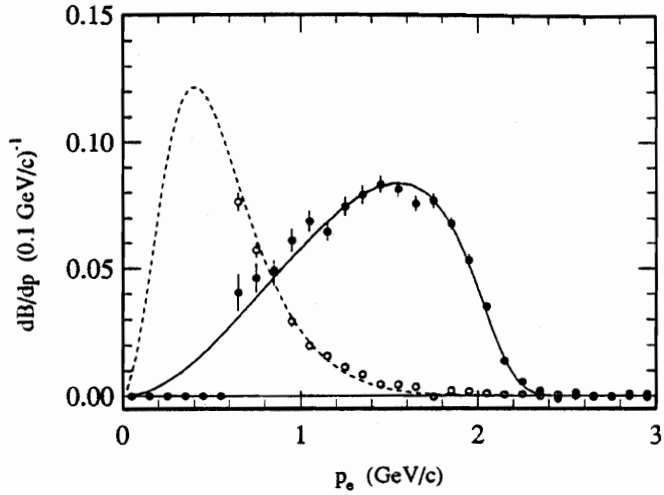

Fig. 14. The lepton momentum spectrum in dilepton events from CLEO. The solid points are for opposite sign leptons, while the open circles indicate like sign lepton pairs. The fit is to the ACM model.

Table 7. V_{cb} Values from Inclusive leptons

Model	Experiment	V_{cb}
ACM	CLEO I	0.042±0.002±0.004
ACM	ARGUS	0.039±0.001±0.003
ACM	CLEO II	0.040±0.001±0.004
ISGW	CLEO I	0.039±0.002±0.004
ISGW	ARGUS	0.039±0.001±0.005
ISGW	CLEO II	0.040±0.001±0.004
ISGW*	CLEO I	0.037±0.002±0.004
ISGW*	CLEO II	0.040±0.002±0.004

statistical and systematic errors for each method linearly. These three numbers are then used in a weighted average to extract

$$|V_{cb}| = 0.0378 \pm 0.0026, \quad \text{and } A = 0.777 \pm 0.053. \tag{24}$$

2.2. The $b \to u$ transistion

2.2.1. Introduction

The only direct experimental evidence for the $b \to u$ transistion is from inclusive $b \to u\ell\nu$ decays, where e^- and μ^- are found beyond the endpoint for $B \to D\ell\nu$ decays. The latest evidence from CLEO II[23] is shown in Fig. 16.

The branching ratios are small. CLEO finds that the rate in the lepton momentum interval $2.6 > p_\ell > 2.4$ GeV/c, $\mathcal{B}_u(p)$, is $(1.5 \pm 0.2 \pm 0.2) \times 10^{-4}$. To extract V_{ub} from this measurement we need to use theoretical models. It is convienent to define: $\Gamma(b \to u\ell\nu) = \gamma_u |V_{ub}|^2$, and $\Gamma(b \to c\ell\nu) = \gamma_c |V_{cb}|^2$. In addition, $f_u(p)$ is the fraction

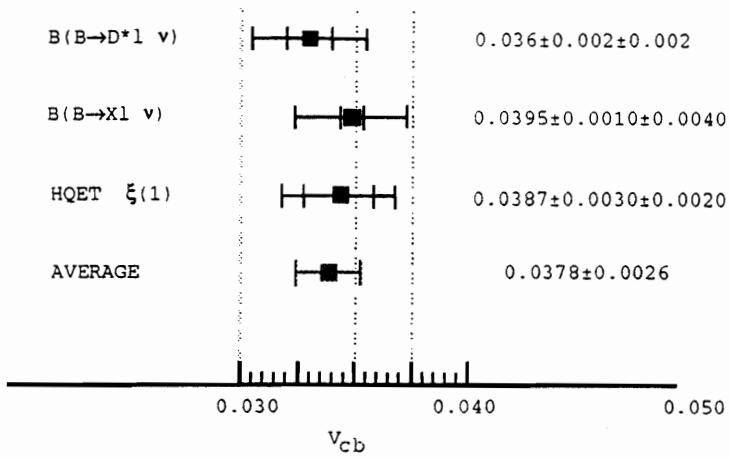

Fig. 15. Summary of $|V_{cb}|$ values found using different methods.

of the spectrum predicted in the end point region by different models, and $\mathcal{B}_{sl}$ is the semileptonic branching ratio. Then:

$$\frac{|V_{ub}|^2}{|V_{cb}|^2} = \frac{\mathcal{B}_u(p)}{\mathcal{B}_{sl}} \cdot \frac{\gamma_c}{f_u(p)\gamma_u}. \tag{25}$$

These models disagree as to which final states populate endpoint region. Most models agree roughly on values of γ_c. However, models differ greatly in the value of the product $\gamma_u \cdot f_u(p)$. There are two important reasons for these differences. First of all, different authors disagree as to the importance of the specific exclusive final states such as $\pi\ell^-\overline{\nu}_\ell$, $\rho\ell^-\overline{\nu}_\ell$ in the lepton endpoint region. For example, the Altarelli et al. model doesn't consider individual final states and thus can be seriously misleading if the endpoint region is dominated by only one or two final states. In fact, several inventors of exclusive models have claimed that the endpoint is dominated by only a few final states.[11,13] Secondly, even among the exclusive form-factor models there are large differences in the absolute decay rate predictions. This is illustrated in Fig. 17. The differences in the exclusive models are much larger in $b \to u$ transitions than in $b \to c$ transitions because the q^2 range is much larger.

Let us return to the question of which final states populate the lepton endpoint region. Ramirez, Donoghue and Burdman[24] claim that the lepton endpoint region is comprised both of exclusive final states and inclusive ones with multiple pions. Their argument is best described by referring to Fig. 18 which shows graphically the $b \to ue\nu$ Dalitz plot. The points labeled (A), (B) and (C) all refer to final state configurations which populate the lepton endpoint region. At point (C) the u-quark is at rest with respect to the intial b-quark and therefore can easily form a hadron with the spectator quark. This region is the one considered in the exclusive models. At point (A) the u-quark has the largest recoil energy but will not, in general, form a single light hadron with the spectator. The entire right hand border is formed by configurations where the three objects are roughly colinear. These considerations have led Ramirez et al. to form a model which has both exclusive and inclusive components.

2.2.2. Value of V_{ub}/V_{cb}

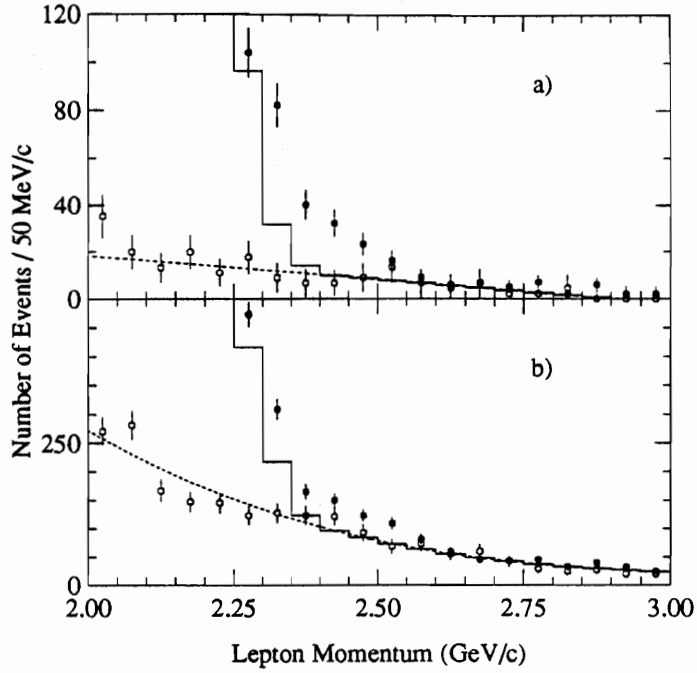

Fig. 16. Lepton yield versus momentum from CLEO II for the "strict" cut sample, $R_2 < 0.2$, $P_{miss} > 1$ GeV/c and the lepton and missing momentum direction point into opposite hemispheres, (a) and the $R_2 < 0.3$ sample (b). The filled points are from data taken on the peak of the $\Upsilon(4S)$, while the open points are continuum data scaled appropriately. The dashed curves are fits to the continuum data, while the solid histograms are predictions of the sum of $b \to c\ell\nu$ and continuum lepton production.

Fig. 19 shows V_{ub}/V_{cb} for different models from an average of data reported by CLEO I,[25] ARGUS[26] and CLEO II[23]. The differences among the models dominates the uncertainty. The best estimate is that V_{ub}/V_{cb}=0.08±0.02.

2.2.3. Limits on exclusive charmless final states

There isn't any convincing evidence for the exclusive final states $\pi\ell\nu$, $\rho\ell\nu$, or $\omega\ell\nu$. The CLEO II upper limits, in WSB model are $\mathcal{B}(B^o \to \pi^-\ell^+\nu) < 4.5 \times 10^{-4}$ and $\mathcal{B}(B^o \to \rho^-\ell^+\nu) < 2.7 \times 10^{-4}$ at 90% confidence level. These give upper limits on V_{ub}/V_{cb} of < 0.18 and < 0.10, respectively.

2.2.4. Constraints on ρ and η

In terms of the Wolfenstein parameters,

$$\left|\frac{V_{ub}}{V_{cb}}\right|^2 = \lambda^2\left(\rho^2 + \eta^2\right), \tag{26}$$

which describes a circle centered at zero in the $\rho - \eta$ plane. From CP violation measurements in neutral kaon decay $\eta > 0$, which lets us describe this constraint as a semiannular region, of radius 0.36±0.09.

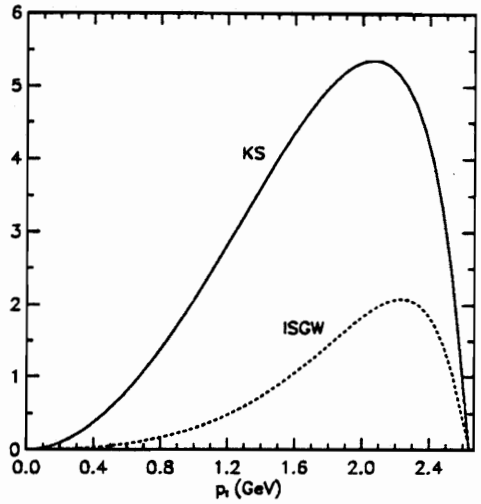

Fig. 17. Lepton momentum spectra for $B \to \pi \ell \nu$ in the KS and ISGW model.

2.3. V_{td}, Information from $B_d^0 - \bar{B}_d^0$ mixing

For $x \equiv \Delta M/\Gamma$, the CKM elements are related to x via

$$x = \frac{G_F^2}{6\pi^2} B_B f_B^2 m_b \tau_B |V_{tb}^* V_{td}|^2 F\left(\frac{m_t^2}{M_W^2}\right) \eta_{QCD}, \tag{27}$$

where G_F is the Fermi constant and f_B is the decay constant of the B meson, which has been calculated theoretically, albeit with very large uncertainty. Since

$$|V_{tb}^* V_{td}|^2 \propto |(1-\rho-i\eta)|^2 = (\rho-1)^2 + \eta^2, \tag{28}$$

the mixing measurement gives a circle centered at (1,0) in the $\rho - \eta$ plane.

The width of the band is caused primarily by the uncertainty in f_B. To measure x experiments have measured the ratio of mixed events to total events either integrating over time, as done by ARGUS and CLEO or recently measuring the explict time dependence, as done by ALEPH and OPAL. One such measurement is shown in Fig. 20. The extracted x values are shown in Table 8.

Table 8. $x = \Delta M/\Gamma$ Values from B_d^0 mixing measurements

Experiment	x
CLEO [27]	0.65±0.10
ALEPH [28]	0.76±0.12
OPAL [29]	0.73±0.14
ARGUS [30]	0.75±0.15
AVERAGE	0.71±0.06

3. What is learned from CP Violation measurments in K_L^0 decay.

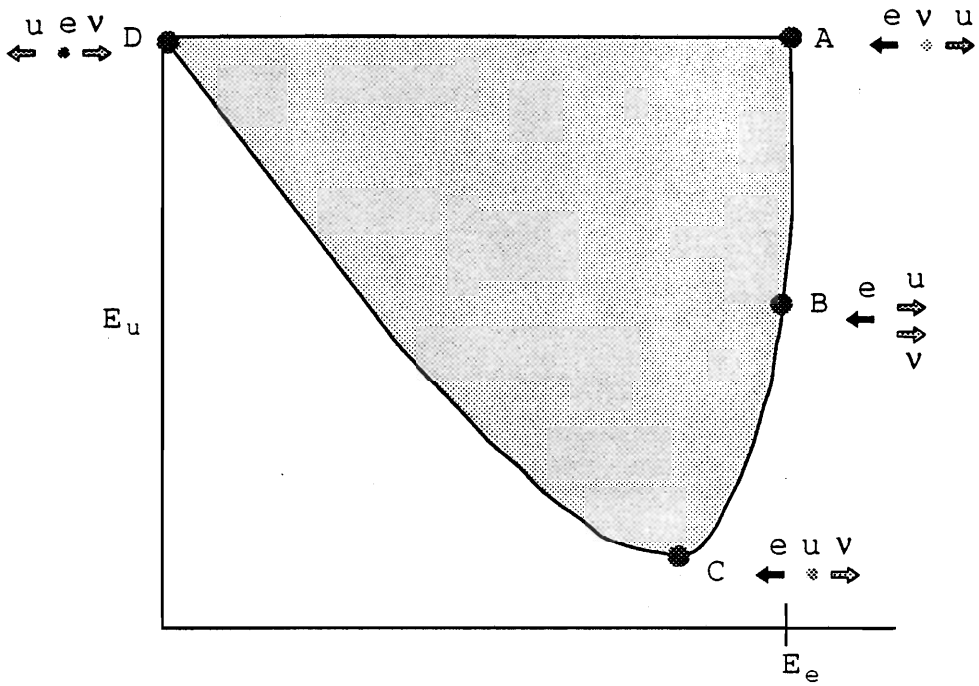

Fig. 18. The Dalitz plot for $b \longrightarrow ue\nu$, with the shaded region being kinematically allowed. Various decay configurations are also shown, including (A), the highest energy point for the electron, and (C), the point with zero hadronic recoil.

The CP violating parameter ϵ is well measured. The constraint equation arising from this measurement is

$$\eta \left[(1-\rho)A^2 + 0.20\right] A^2 \frac{B_K}{0.65} = 0.15, \tag{29}$$

where B_K is a parameter which is related to the probability that the s and d quarks form a neutral K meson. This parameter must be calculated from theory. (Note also, that the numbers 0.20 and 0.15 depend somewhat on the charm quark and top quark masses.) The predictions of B_K are given in Fig. 21.

Following Buras and Harlander,[31] I take $B_K = 0.65 \pm 0.15$. The constraints in the $\rho - \eta$ plane from $|V_{ub}/V_{cb}|$, B mixing and ϵ are shown in Fig. 22. I use $240 > f_B > 160$ MeV, which gives a range consistent with most calculations, and will be discussed later.

The bands are shown with one standard deviation error bars. The consistency between all three measurements is remarkable. While it is of utmost importance to reduce the errors on all of these measurements, presently the Standard Model is spot on.

The error sources for the ϵ constraint are shown in Fig. 23. The largest error arises from the error on the A parameter, which results from the A^4 dependence. The error on B_K is also important. It is interesting that the uncertainty due to the error on m_t already is smaller than these other sources.

4. Meson Decay Constants

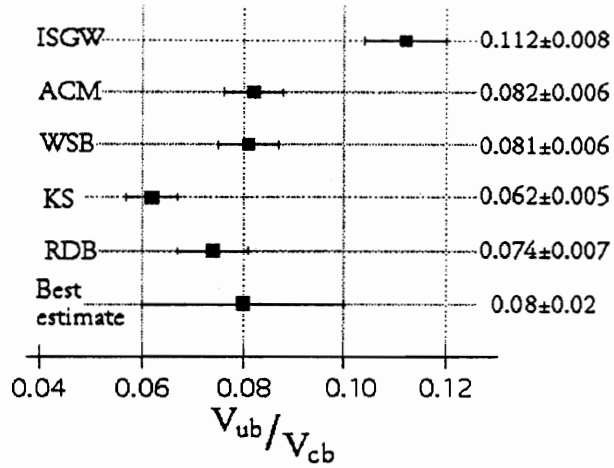

Fig. 19. $|V_{ub}/V_{cb}|$ from an average of CLEO I, ARGUS and CLEO II measurements using different models.

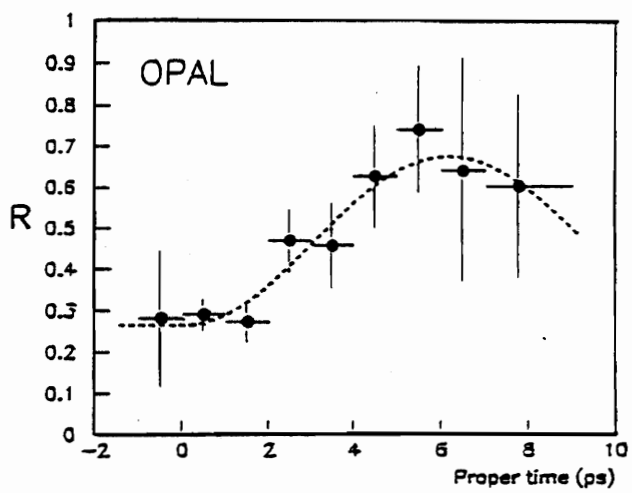

Fig. 20. The ratio R of mixed B events as a function of time.

4.1. Introduction

Purely leptonic decays of pesudoscalar mesons (P) can occur, and this is by far the best way to measure the decay constants. The example of $\pi^- \to \mu^-\bar{\nu}$, is shown in Fig. 24. The mechanism is that the quark (Q) and antiquark ($\bar{q}$) annihilate via the charged current. The probability that this occurs is proportional to the wave function overlap and this information is contained in the "decay constant," f_P, in the expression

$$\Gamma(P^+ \to \ell^+\nu) = \frac{1}{8\pi} G_F^2 f_P^2 m_\ell^2 M_P \left(1 - \frac{m_\ell^2}{M_P^2}\right)^2 |V_{Qq}|^2. \tag{30}$$

Since all the terms except f_P are known, a measurement of the partial decay width serves to determine f_P. In fact, this has been done for π^-, K^-, and D_s^+ mesons. For D^+ and the important B^- mesons there are only upper limits. The experimental

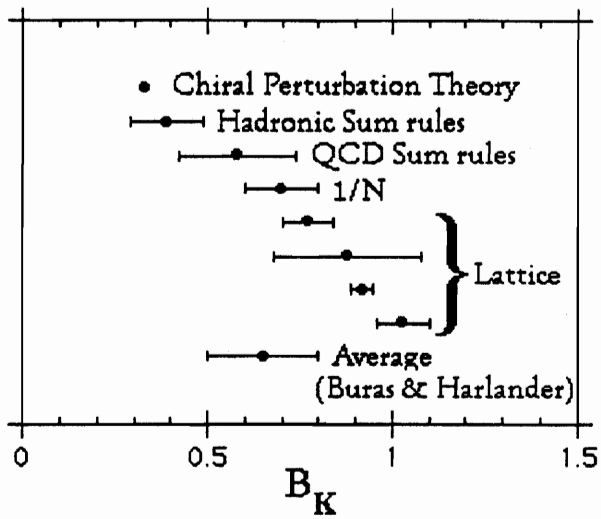

Fig. 21. Values of B_K calcualted in different models.

situation is given in Table 9. [3,32]

Table 9. Measured Decay constants

Particle	f_P
π^-	131.73±0.15 MeV
K^-	160.6±1.3MeV
D_s^+	344±76 MeV
D^+	<290 MeV (@ 90% c.l.)
B^-	<1200 MeV (@ 90% c.l.)

It is extremely difficult to measure the leptonic decay widths of the B^- or even the D^+ or D_s^+. For an f_P of 250 MeV, I show in Fig. 25 the expected branching ratios into either electrons, muons or τ's for these particles. The D_s^+ has the largest branching ratios. Even the $\mu^+\nu$ rate is close to 1%. The branching ratio for the D^+ is suppressed by a factor of 20 due to the CKM element $|V_{cd}|^2$, while the B^- is suppressed even more, by $|V_{ub}|^2$. Note also that in this process lepton universality is badly broken, due to the lepton mass terms in Eq. (30), above. The electron rate is suppressed so much compared to the muon rate, that the electron channel can be used as a background estimator.

4.2. The CLEO f_{D_s} measurement

I will now describe the CLEO measurement of f_{D_s}. CLEO looks for the decay sequence $D_s^{*+} \to \gamma D_s^+$, with the subsequent decay $D_s^+ \to \mu^+\nu$. The basic technique used is to detect the γ and the μ^+, and use the measurement of the missing momentum and energy to "detect" the neutrino. Then the difference in invariant mass is calculated as

$$\Delta M = M(\gamma\mu^+\nu) - M(\mu^+\nu). \tag{31}$$

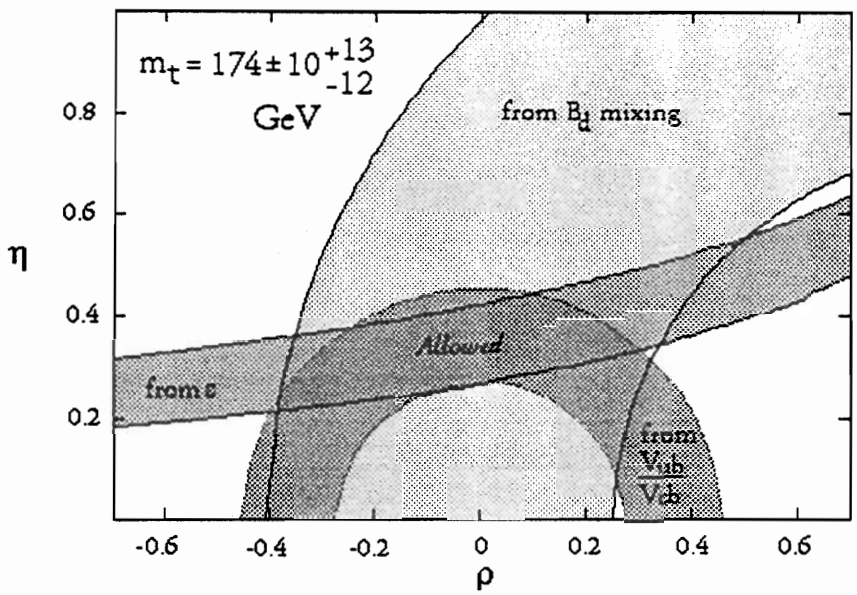

Fig. 22. Constraints in the $\rho - \eta$ plane from $|V_{ub}/V_{cb}|$, $B_d^0 - \bar{B}_d^0$ mixing and CP violation in the K_L^0 system (ϵ). The bands are $\pm 1\sigma$.

The physics backgrounds are measured by looking for the vanishingly small process with an electron in the final state. This requires precise knowledge of the relative muon/electron efficiencies and fake rates.

The detection efficiency and signal shape are measured directly from the data using the similar process $D^{*0} \to \gamma D^0$, with the subsequent decay $D^0 \to K^-\pi^+$. After this sample is selected, the detector measurements of the π^- are removed and the K^+ is called the μ^+. (Use of missing momentum and energy to determine the π^- four-vector is denoted by $\not{\pi}^-$.) They also use, for some purposes, a sample of $D^{*+} \to \pi^+ D^0$, with the subsequent decay $D^0 \to K^-\pi^+$.

The signal shape is measured using the D^{*o} sample and computing the mass difference

$$\Delta M = M(\gamma\mu^+\nu) - M(\mu^+\nu) = M(\gamma K^+\not{\pi}^-) - M(K^+\not{\pi}^-), \tag{32}$$

after requiring that 2.6 GeV$> M(K^+\not{\pi}^-) >$ 1.6 GeV. The resulting signal shape is shown in Fig. 26(a). Besides D_s^{*+} signal events there are other sources of $\mu^+\nu$ events in the ΔM distribution. These include D_s^{*+} events where the real γ is replaced with a random one, and direct D_s^+ decays which pair with a random γ. These contributions are simulated using the D^{*+} sample. The resulting ΔM distribution using tagged D^{*+} is shown in Fig. 26(b). The CLEO data is shown in Fig. 27. CLEO finds 39±8 D_s^{*+} and 54±11 D_s^+ events. They normalize to the relatively prolific $\phi\pi^+$ decay mode, and find

$$\frac{\Gamma(D_s^+ \to \mu^+\nu)}{\Gamma(D_s^+ \to \phi\pi^+)} = 0.245 \pm 0.052 \pm 0.074. \tag{33}$$

The systematic errors are given in Table 10. To extract a value of f_{D_s}, we need to know the value of $\mathcal{B}(D_s \to \phi\pi^+)$. CLEO uses (3.7±0.9)% from assuming that

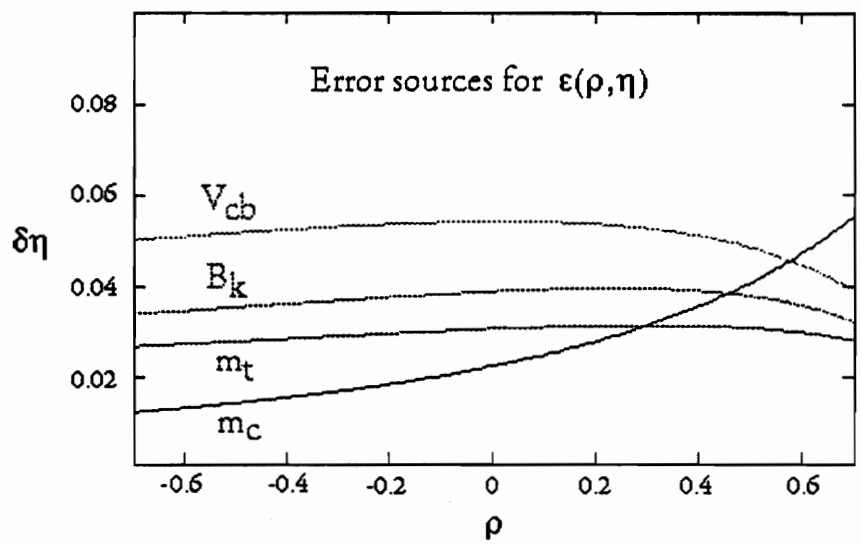

Fig. 23. The contributions to the error on the ϵ constraint as a function of ρ.

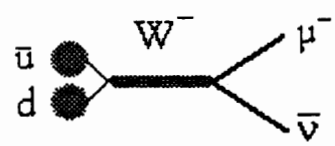

Fig. 24. Quark level diagrm of π^- decay.

$\Gamma(D \to K^* \ell^+ \nu)$ is nearly equal to $\Gamma(D_s \to \phi \ell^+ \nu)$. The resulting value is:

$$f_{D_s} = (344 \pm 37 \pm 52 \pm 42) \text{ MeV}, \tag{34}$$

where the first error is statistical, the second systematic and the third arises from the error in the $\phi\pi^+$ branching ratio.

4.3. Other estimates of $\mathcal{B}(D_s \to \phi\pi^+)$

Since the value used for $\mathcal{B}(D_s \to \phi\pi^+)$ is important for arriving at a final result, I now update an analysis by Muheim and Stone.[33] They derived values in three different way, the first of which is the same as used by CLEO, and described above. In the second method they make use of the fact that the particle known as the D_s^{**+} of mass 2536 MeV decays into D mesons rather than D_s mesons. The method works in the following way: since we know, in continuum e^+e^- annihilations, the production cross-sections for D^0 and D^+ mesons and the product of the cross-section times branching ratio for $D_s \to \phi\pi^+$, then if we knew the relative probability of popping an $s\bar{s}$ pair rather than a $u\bar{u}$ or $d\bar{d}$ pair, we could easily compute the $\phi\pi^+$ branching ratio. We know the cross-sections for production of both the $J^P = 1^+$ D^{**} and D_s^{**+}. These can be found because $D^{**} \to D^*\pi$, and $D_s^{**} \to D^*K$. Since the ratio of the production cross-sections is proportional to the relative popping probability of $s\bar{s}$, this measurement results in an estimate of

$$\mathcal{B}(D_s \to \phi\pi^+) = (4.6 \pm 1.5)\%. \tag{35}$$

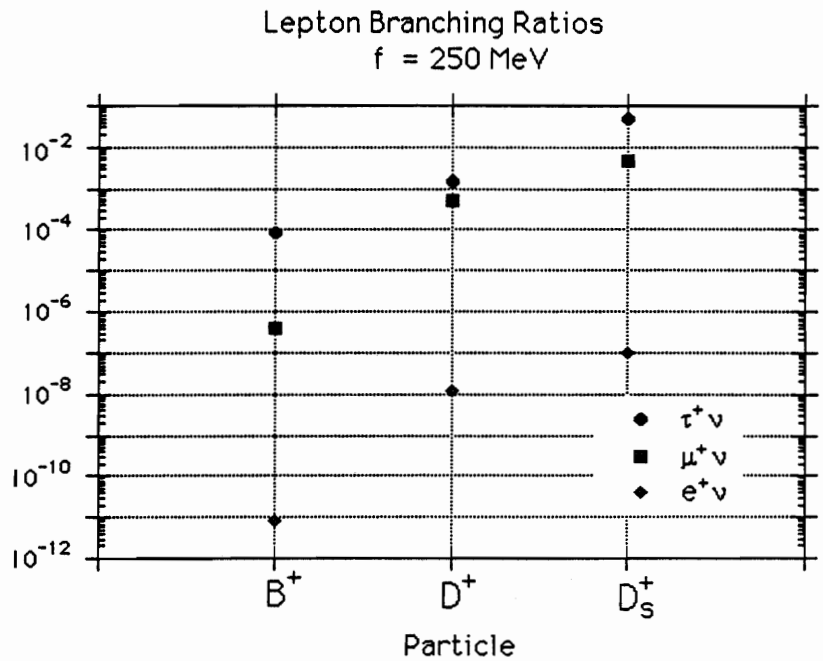

Fig. 25. The branching ratio for purely leptonic decays of B^+, D^+, D_s^+ mesons, assuming f_P equals 250 MeV.

The third technique uses the assumption of factorization in B decays. Factorization has been used with different meanings. The definition used here is that the matrix element can be written as a product of two currents, similar to semileptonic decays (See Eq. (5).) Thus the decay $B \to D^* D_s$ is the product of a current describing the $B \to D^*$ transistion, with one describing the virtual W^- to D_s coupling. The latter is described by f_{D_s}, while the former can measured using $B \to D^* \ell \bar{\nu}$.[34] Explicitly:

$$\frac{\Gamma(B \to D^* D_s^-)}{\frac{d\Gamma}{dq^2}(B \to D^* \ell \bar{\nu})|_{q^2=m_{D_s}^2}} = \delta \times 6\pi^2 |V_{cs}|^2 f_{D_s}^2. \tag{36}$$

δ reflects the fact that in the semileptonic decay all three helicity amplitudes for the $B \to D^*$ matrix element are allowed, while for the pseudoscalar vector final state given here only the longitudinally polarized state is allowed; δ is taken as 0.41. We can also apply this formula to the hadronic final state $D^* D_s^*$. In that case in the right hand side of Eq. (36) δ becomes one and $f_{D_s}^2$ is replaced with $f_{D_s^*}^2$. For the remainder of this treatment, it is assumed that f_{D_s} equals $f_{D_s^*}$. Some authors have argued that there is an additional factor multiplying the right hand side, which allows for a violation of factorization of about 10%.[35] However, the spirit of this approach is to assume that factorization holds exactly.

For this particular analysis it is possible to use both charged and neutral B mesons, since only the simple spectator diagram (see Fig. 8.) can produce these semileptonic or hadronic decays. Although there is hadronic data on DD_s as well as $D^* D_s$ final states, the former are not used due to the lack of corresponding semileptonic data.

Use of the CLEO II data given in Table 11, allows one to solve for f_{D_s} in terms of known quantities as a function of $\mathcal{B}(D_s \to \phi\pi^+)$. Averaging over both D_s and D_s^*

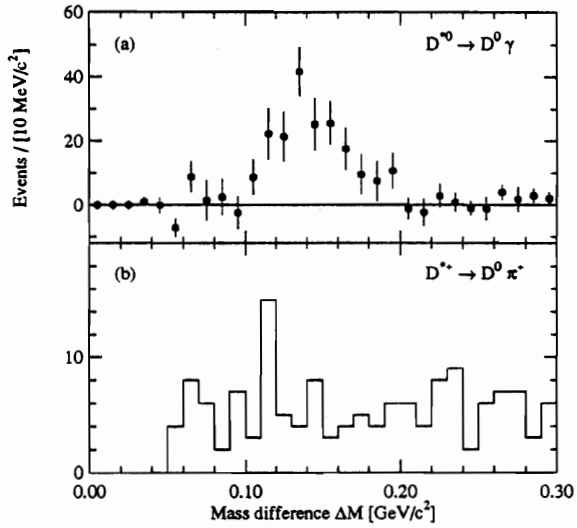

Fig. 26. The mass difference distributions for (a) the $D^{*0} \to \gamma D^0$, $D^0 \to K^-\pi^+$ event sample, eliminating the the π^+ and using missing momentum analysis. (b) The $D^{*+} \to \pi^+ D^0$, $D^0 \to K^-\pi^+$ event sample using missing momentum analysis and combining with random photons.

Table 10. Systematic errors on f_{D_s}

Source of Error	Value	Size of error (%)
μ fake rate	(0.61±0.14)%	19
e fake rate	(0.30±0.07)%	9
μ/e normalization	1.94±0.05%	11
Detection efficiency	(2.5±0.4)%	13
D_s^*/D_s ratio	1.03±0.20	11
$\phi\pi^+$ normalization	5779±436±405	6
Total		30

modes, the equation is:

$$f_{D_s} = (280 \pm 43)\sqrt{\frac{3.7\%}{\mathcal{B}(D_s \to \phi\pi^+)}}\text{MeV}. \tag{37}$$

The CLEO II detection of $D_s \to \mu\nu$ can be expressed as

$$f_{D_s} = (344 \pm 64)\sqrt{\frac{\mathcal{B}(D_s \to \phi\pi^+)}{3.7\%}}\ \text{MeV}. \tag{38}$$

Solving the two equations gives

$$f_{D_s} = (310 \pm 37)\ \text{MeV}, \quad \text{and } \mathcal{B}(\text{D}_s \to \phi\pi^+) = (3.0 \pm 0.7)\%. \tag{39}$$

Yet another indirect method is based on assuming that $\Gamma(D \to X\ell^+\nu)$ is nearly equal to $\Gamma(D_s \to X\ell^+\nu)$. CLEO uses their measurement of $\mathcal{B}(D^0 \to X\ell^+\nu)$ and

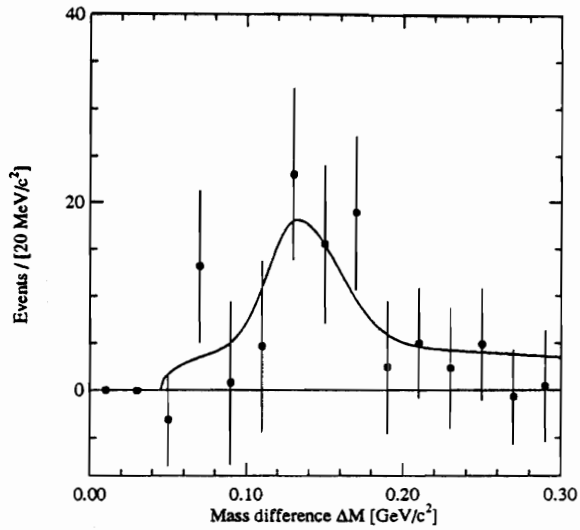

Fig. 27. The mass difference distributions for D_s^{*+} candidates, with all backgrounds subtracted.

Table 11. CLEO II data on $D^* D_s$ modes

Mode	$\mathcal{B}$
$\mathcal{B}(B \to D^* D_s)$	$(1.07 \pm 0.23 \pm 0.23)\ \frac{3.7\%}{\mathcal{B}(D_s \to \phi\pi^+)}$
$\mathcal{B}(B \to D^* D_s^*)$	$(1.98 \pm 0.42 \pm 0.45)\ \frac{3.7\%}{\mathcal{B}(D_s \to \phi\pi^+)}$
$\frac{d\mathcal{B}}{dq^2}(B \to D^* \ell\bar{\nu})\|_{q^2=m_{D_s}^2}$	$(5.0 \pm 0.7) \times 10^{-3} GeV^{-2}$

their new branching ratio measurements for the D_s^+ exclusive semileptonic final states $\eta\ell^+\nu$, $\eta'\ell^+\nu$, and $\phi\ell^+\nu$. [36] They then get the inclusive D_s semileptonic branching ratio by summing these three modes and adding in a correction for Cabibbo suppressed modes (5%) and other not yet seen modes (6%). They estimate $\mathcal{B}(D_s^+ \to \phi\pi^+) = (3.82 \pm 0.74)\%$.

The results for $\mathcal{B}(D_s \to \phi\pi^+)$ are shown in Fig. 28, as well as an upper limit derived from counting all the seen decays. The average value is 3.6±0.4%. Using this value the measured CLEO result becomes

$$f_{D_s} = (340 \pm 37 \pm 52 \pm 19)\ \text{MeV}. \tag{40}$$

4.4. Other results on f_P

Although larger than the Mark III upper limit derived from D^+ decay of $f_D < 290$ MeV,[37] the CLEO result is consistent since $f_{D_s}/f_D \approx 1.1$ from theoretical considerations. The CLEO result is higher than the WA75 result based on 6 events of (232± 45 ±20 ±48) MeV.[38] However, this experiment had no measured normalization modes and relied on extrapolations of the D_s production cross section from other nuclear targets at different energies. They used the current PDG average at the time of their publication that $\mathcal{B}(D_s \to \phi\pi^+) = 2.8\%$.

Comparisons with theoretical models are given in Table 12.

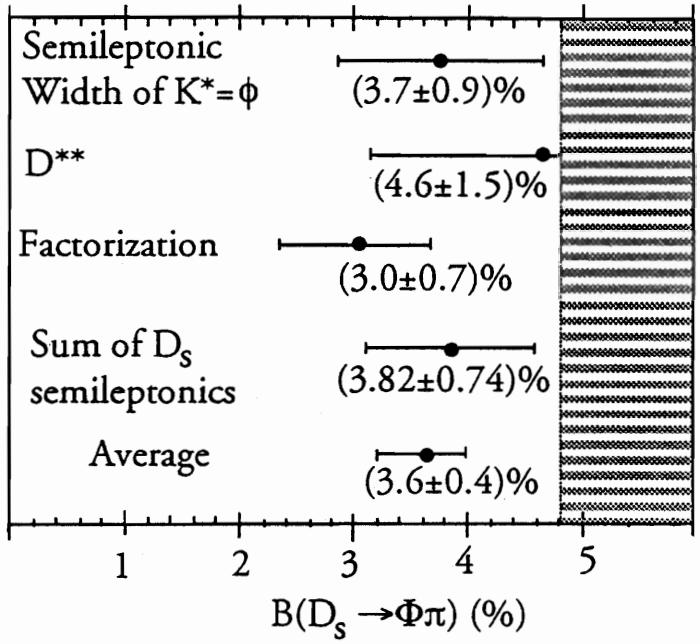

Fig. 28. Summary of $\mathcal{B}(D_s^+ \to \phi\pi^+)$ branching ratio estimates. The shaded region is excluded at 90% c.l.

The CLEO measurement of f_{D_s} is higher than most theoretical predictions. This favors larger values for f_B and, as we will see later, large CP asymmetries in B decays.

5. The unitarity triangle

5.1. Introduction

Since the CKM matrix is unitary we can multiply any row or any column by the complex conjugate of another row or column. The most useful such relationship is:

$$\begin{aligned} V_{td} \cdot V_{ud}^* + V_{ts} \cdot V_{us}^* + V_{tb} \cdot V_{ub}^* &= 0 \\ \text{or } V_{td} + V_{ts} \cdot \lambda + V_{ub}^* &= 0 \\ V_{td} - A\lambda^3 + V_{ub}^* &= 0 \\ V_{td}/A\lambda^3 + V_{ub}^*/A\lambda^3 &= 1 \end{aligned} \tag{41}$$

Think of this as a vector equation with each "vector" representing the sides of a triangle.

The magnitudes of the sides are:

$$\begin{aligned} 1 & \\ V_{td}/A\lambda^3 &= \frac{1}{\lambda}\sqrt{(\rho-1)^2+\eta^2)} = \frac{1}{\lambda}V_{td}/V_{ts} \\ V_{ub}^*/A\lambda^3 &= \frac{1}{\lambda}\sqrt{\rho^2+\eta^2)} = \frac{1}{\lambda}V_{ub}/V_{cb} \end{aligned} \tag{42}$$

A triangle consistent with the data is shown in Fig. 29, where the angles α, β and γ are defined.

Table 12. Theoretical predictions of f_{D_s} and f_B

Model	f_{D_s} MeV	f_B MeV
Lattice[39]		
Bernard , Shen , Soni	230±35	187±37
Gavela et al.	215±17	120
ELC	230±20	157-205
UKQCD	≈211	
DeGrand and Loft	222±16	
Potential[40]		
Sinha	356	229
Cea et al.	141	163
Capstick and Godfrey	290±20	155±15
QCD sum rules[41]		
Narison	154±29	132±17
Shifman	200±15	115±15
Dominguez Paver	194±12	104-150

5.2. To test the Standard Model

We can measure all 3 sides AND all 3 angles. If we see consistency between all of these measurements we have defined the parameters of the Standard Model. If we see inconsistency the breakdown can point us to a more complete theory.

We know two sides already. The base is defined as 1, and the leftmost side comes from $|V_{ub}/V_{cb}|$. The righmost side can be found using $B^0 - \bar{B}^0$ mixing. As we have seen this introduces a large error due to f_B uncertainty. There are two solutions to this problem.

One solution is to measure B_s^0 mixing. The ratio between x_s and x is given by

$$\frac{x_s}{x} = \left(\frac{B_s}{B}\right)\left(\frac{f_{B_s}}{f_B}\right)^2\left(\frac{\tau_{B_s}}{\tau_B}\right)\left|\frac{V_{ts}}{V_{td}}\right|^2, \tag{43}$$

The ratios of the B parameters and decay constants are much better known than the absolute values. The allowed values for x_s as a function of ρ are given in Fig. 30.

The second method for finding the rightmost side of the triangle is to use the measurement of V_{td}/V_{ts} from "Penguin" diagrams. CLEO found the first unambiguous evidence for such graphs by finding the decay $B \to K^*\gamma$.[42] The diagram for this process is shown in Fig. 31. Recently they have also measured the inclusive rate $\mathcal{B}(b \to s\gamma) = (2.3 \pm 0.5 \pm 0.4) \times 10^{-4}$.[43]

If the ts vertex in Fig. 31 where to be replaced with a td vertex, the final state would be $\rho\gamma$. Therefore a measurement of the relative rates

$$R_p = \mathcal{B}(B \to \rho\gamma)/\mathcal{B}(\to K^*\gamma) = \zeta|V_{td}/V_{ts}|^2, \tag{44}$$

where ζ is a model dependent correction due to different form-factors for the K^* and the ρ. Current models predict $\zeta = 0.58, 0.77, 0.81$. The CLEO II data[44] are shown in Fig. 32, from which it is found that $R_p < 0.34$ @ 90 % c. l. This is far from the

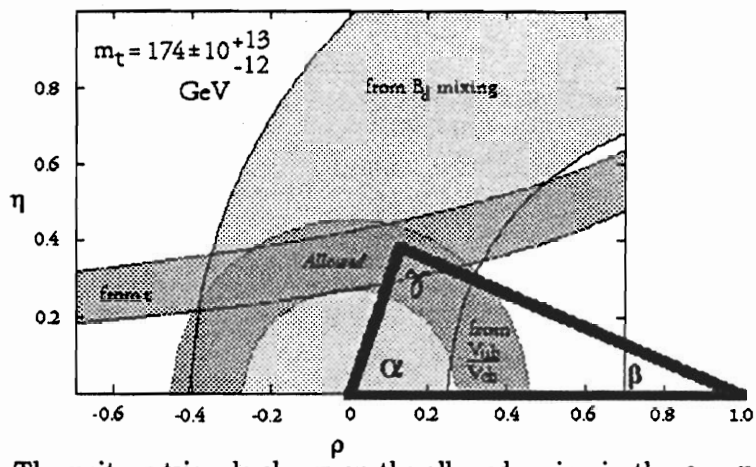

Fig. 29. The unitary triangle shown on the allowed region in the $\rho - \eta$ plane.

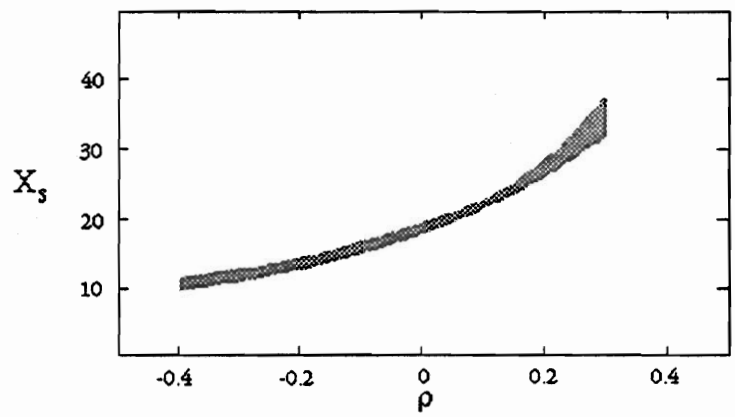

Fig. 30. The allowed values for x_s as a function of ρ.

range suggested from our allowed region in the $\rho - \eta$ plane, which is $0.07 > R_p > 0.02$ for ζ of 0.7. The upper value is for ρ of -0.040, while the lower value is for ρ of 0.30. A. Soni has claimed that "long distance" effects may pollute this measurement.[46]

5.3. Measure angles using CP violation

There are several ways of measuring CP violation in B decays. All of them rely on the interference between two amplitudes. In the "classic" case, CP violation via $B^0 - \overline{B}^0$ mixing, we choose a final state which is accessible to both B^0 and $\overline{B}^0$ decays. The second amplitude necessary for interference is provided by mixing as depicted in Fig. 33.

At the $\Upsilon(4S)$, $e^+e^- \to \gamma \to B^0\overline{B}^0$, which is a state of negative charge conjugation. For final states which are CP eigenstates an asymmetry exists, but its time integral is zero. Therefore we need to make time dependent measurments, which can be done by using asymmetric beam energies in order to get the B's moving. An alternative is to measure the process $e^+e^- \to \gamma \to B^0\overline{B}^0\gamma$, which is a C=+1 final state.[47] However,

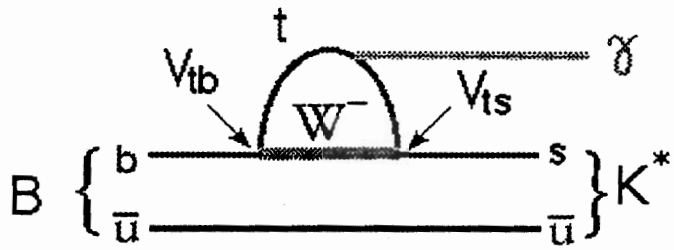

Fig. 31. Loop diagram for $B \to K^*\gamma$.

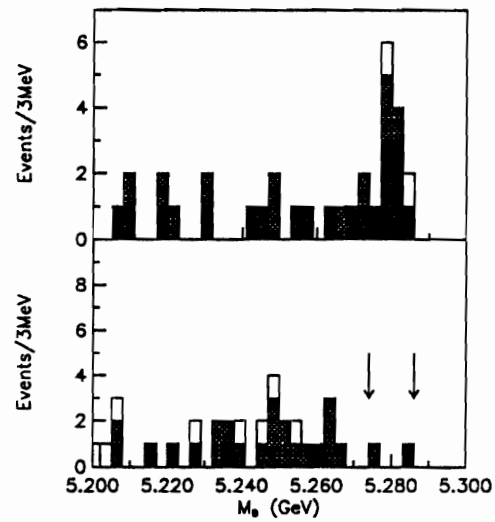

Fig. 32. The B candidate mass distributions for $K^*\gamma$ (top) and $(\rho + \omega)\gamma$ (bottom). The bottom plot includes 50% more integrated luminosity than the top. The arrows indicate the signal region. The dark entries for the upper (lower) plot are the $K^-\pi^+$ ($\pi^-\pi^+$) events, the cross-hatched $K^-\pi^0$ ($\pi^-\pi^0$), and the white $K_s^0\pi^+$ ($\pi^-\pi^+\pi^0$).

the measured cross section is down by factor of 7 with respect to the $\Upsilon(4S)$.[48] Another alternative is to use a hadron collider. The Main Injector at FNAL will produce 1000 times as many B's as an e^+e^- machine.

Examples of final states most discussed to measure CP violation via mixing are ψK_s which measures the angle 2β, and $\pi^+\pi^-$ which measures the angle 2α.

Interference can also arise between "Penguin" and "Tree" graphs. In this case we have two distinct processes which yield the same final state so they interfere. This can lead to a rate asymmetry between B^- and B^+. An example is the decay $B^- \to K^-\pi^0$, depicted in Fig. 34.

Gronau, Rosner and London have[49] shown using the assumption of SU(3) and isospin relations that this mode coupled with a study of $B^- \to \pi^-\pi^0$ and $B^- \to \pi^-K^0$ can be used to measure the angle γ independent of any hadronic matrix elements. There is a similar plan using the decays $B^- \to D^0K^-$, $\overline{D}^0K^-$ and $D^0_{CP}K^-$, where D^0_CP indicates the decay into a CP eigenstate.[50]

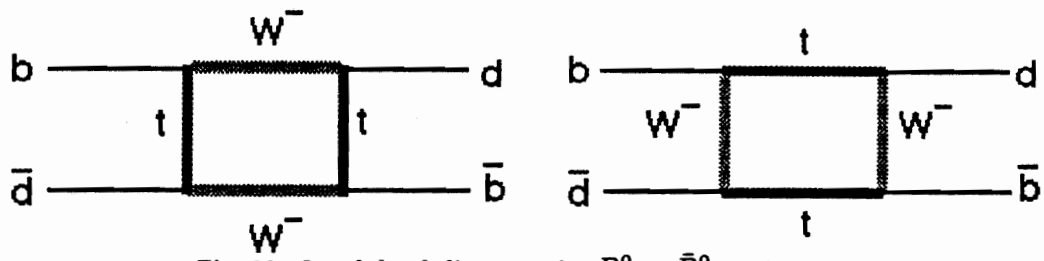

Fig. 33. Quark level diagrams for $B^0 - \bar{B}^0$ mixing.

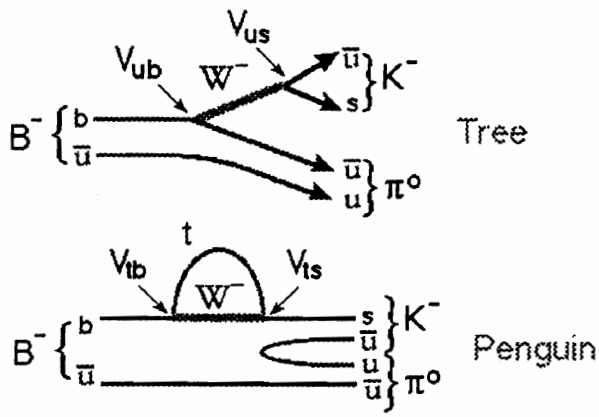

Fig. 34. Tree level $b \longrightarrow u$ diagram and loop diagram for the final state $K\pi$.

5.4. Predictions of CP violating angles

The preferred range of CP violating angles as a function of the CKM parameter ρ is shown in Figs. 35, 36, 37. It should be kept in mind that ρ is closely related to f_B, so that negative ρ corresponds to small values of f_B, while positive ρ corresponds to large values. I have plotted the variables $sin(2\alpha)$, $sin(2\beta)$, and $sin(\gamma)$, since these are directly related to the asymmetries that can be measured in the methods mentioned here. Large asymmetries are expected for the last two (2β, γ), while the first, (2α) can have almost any asymmetry.

6. Conclusions

The CKM model is consistent with data on V_{ub}/V_{cb}, $B^0 - \overline{B}^0$ mixing and the value of ϵ from CP violation in the kaon system, for a heavy top quark. Specifically,

- $|V_{cb}| = 0.038 \pm 0.003 \Rightarrow \; A = 0.78 \pm 0.06$
- $\left|\frac{V_{ub}}{V_{cb}}\right| = 0.08 \pm 0.02, \Rightarrow \; |V_{ub}| = 0.0030 \pm 0.0008$
- $f_{D_s} = (344 \pm 37 \pm 52 \pm 19)$ MeV
- Large CP violating asymmetries are expected in B decays

7. Acknowledgements

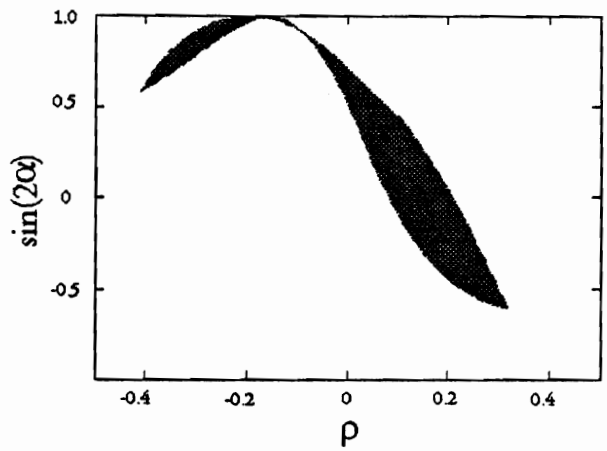

Fig. 35. Allowed region of $sin(2\alpha)$ versus ρ.

I thank A. Ali, J. Rosner, A. Soni, M. Artuso, F. Muheim and S. Playfer for useful discussions. This work was supported by the National Science Foundation.

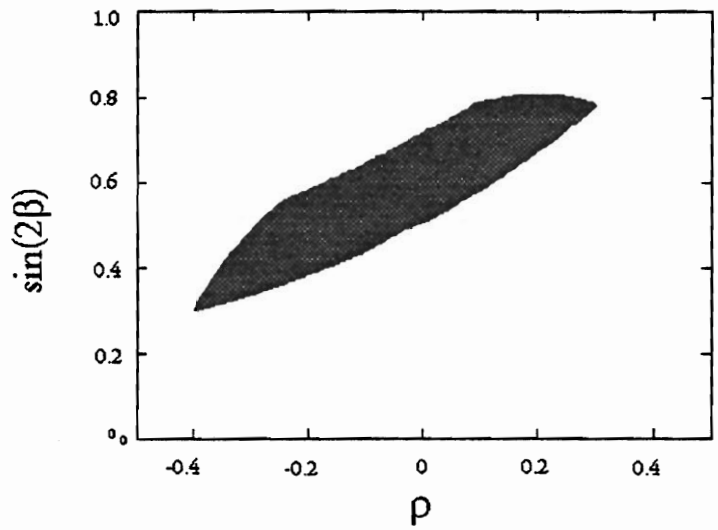

Fig. 36. Allowed region of $sin(2\beta)$ versus ρ.

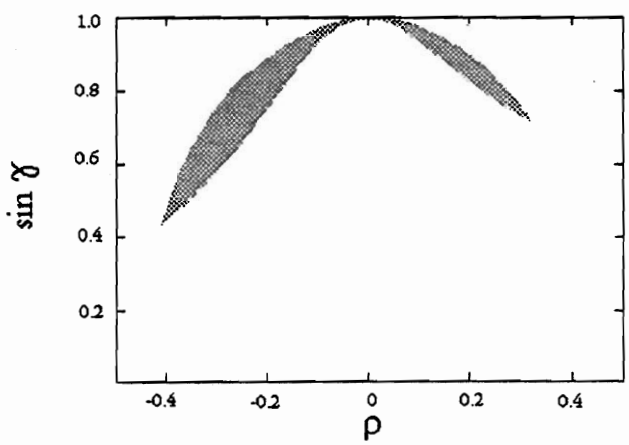

Fig. 37. Allowed region of $sin(\gamma)$ versus ρ.

8. References

[1] L. Wolfenstein, Phys. Rev. D **31**, 2381 (1985).

[2] A. Ali, "*B* Decays - Introduction and Overview," in *B Decays 2nd edition*, ed. S. Stone, World Scientific, Singapore (1994), and references contained therein.

[3] L. Montanet et al., (Particle Data Group) Phys. Rev. D **50**, 1173 (1994).

[4] K. Kleinknecht in *CP Violation*, ed. C. Jarlskog, World Scientific, Singapore (1989), p 41.

[5] See F. J. Gilman and R. L. Singleton,Phys. Rev. D **41**, 142 (1990);K. Hagiwara, A. D. Martin and M. F. Wade Nucl. Phys. **B327**, 569 (1989); S. Stone "Semileptonic *B* Decays," in *B Decays 2nd edition*, ed. S. Stone, World Scientific, Singapore (1994).

[6] D. Bortoletto et al., (CLEO) Phys. Rev. Lett. **16**, 1667 (1989).

[7] H. Albrecht et al., (ARGUS) Zeit. Phys. C **57**, 533 (1993).

[8] H. Albrecht et al., (ARGUS) Phys. Lett. B **275**, 195 (1992).

[9] B. Barish et al., (CLEO II) CLNS 94/1285 (1994).

[10] W. Venus, "*b* Weak Interaction Physics at High Energies," in proc. of XVI Int. Symp. on Lepton-Photon Interactions, ed. P. Drell and D. Rubin, AIP Press, NY (1993).

[11] N. Isgur, D. Scora, B. Grinstein, and M. B. Wise, Phys. Rev. D **39**, 799 (1989).

[12] J. G. Korner and G. A. Schuler, Zeit. Phys. C **38**, 511 (1988); ibid, (erratum) **C41**, (1989), 690.

[13] M. Wirbel, B. Stech and M. Bauer, Zeit. Phys. C **29**, 637 (1985); M. Bauer and M. Wirbel, Z. Phys. **C42**, 671(1989).

[14] W. Jaus, Phys. Rev. D **41**, 3394 (1990).

[15] N. Isgur and M. B. Wise, Phys. Lett. B **232**, 113 (1989), ibid Phys. Lett. B **237**, 527 (1990).

[16] M. Neubert, SLAC-PUB-6263, to appear in Physics Reports; A. Falk, M. Neubert and M. Luke, Nucl. Phys. **B388**, 3363 (1992); A. Falk and M. Neubert, Phys. Rev. D **47**, 2965 (1993); M. Neubert, Phys. Rev. D **47**, 4063 (1993); M. Neubert and V. Rieckert, Phys. Lett. B **382**, 97 (1992); M. E. Luke, Phys. Lett. B **252**, 447 (1990).

[17] M. Shifman, N. Uraltsev and A. Vainshtein, Univ. of Minn. preprint TPI-MINN-94/13-T (1994).

[18] A new value of $\xi(1)$ from Neubert of 0.93 ± 0.03 is consistent with the average value used here. M. Neubert, "Theoretical Update on the Model-Independent Determination of $|V_{cb}|$ Using Heavy Quark Symmetry," CERN-TH.7395/94 (1994).

[19] G. Altarelli, N. Cabibbo, G. Corbo and L. Maiani, Nucl. Phys. **B207**, 365 (1982).

[20] J. Bartelt et al. (CLEO), " Inclusive Measurements of B-meson Semileptonic Branching Fractions," submitted to Lepton Photon conf., Cornell (1993), CLEO-CONF 93-19.

[21] H. Albrecht et al., (ARGUS) Phys. Lett. B **318**, 397 (1993).

[22] J. Gronbert et al., (CLEO) "Measurement of the Branching Ratio $B \to Xe\nu$ with Lepton Tags," CONF 94-6.

[23] J. Bartelt et al., (CLEO) Phys. Rev. Lett. **71**, 4111 (1993).

[24] C. Ramirez, J. F. Donoghue and G. Burdman, Phys. Rev. D **41**, 1496 (1990).

[25] R. Fulton et al., (CLEO) Phys. Rev. Lett. **64**, 16 (1990).

[26] H. Albrecht et al., (ARGUS) Phys. Lett. B **234**, 409 (1990).

[27] J. Bartelt et al., (CLEO) Phys. Rev. Lett. **71**, 1680 (1993).

[28] D. Buskulic et al., (ALEPH) Phys. Lett. B **322**, 441 (1994).

[29] R. Akers et al., (OPAL) Zeit. Phys. C **60**, 199 (1993).

[30] H. Albrecht et al., (ARGUS) Zeit. Phys. C **55**, 357 (1992).

[31] A. Buras and M. Harlander, "A Top Quark Story: Quark Mixing, CP Violation and Rare Decays in the Standard Model," in *Heavy Flavours*, ed. A. Buras and M. Linder, World Scientific, Singapore (1992).

[32] J. Alexander et al., (CLEO) "A Search for $B \to \tau\nu$," CONF 94-5

[33] F. Muheim and S. Stone, Phys. Rev. D **49**, 3767 (1994).

[34] J. L. Rosner, Phys. Rev. D **42**, 3732 (1990); D. Bortoletto and S. Stone, Phys. Rev. Lett. **65**, 2951 (1990).

[35] M. Dugan and B. Grinstein, Phys. Lett. B **255**, 583 (1991).

[36] M. Battle et al., (CLEO), "Measurement of the ratios $\mathcal{B}(D_s^+ \to \eta\ell^+\nu)/\mathcal{B}(D_s^+ \to \phi\ell^+\nu)$, and $\mathcal{B}(D_s^+ \to \eta\ell^+\nu)/\mathcal{B}(D_s^+ \to \phi\ell^+\nu)$," CONF 94-18 (1994).

[37] J. Adler (Mark III), Phys. Rev. Lett. **60**, 1375 (1988), erratum ibid, **63**, 1658 (1989).

[38] S. Aoki et al., Progress of Theoretical Physics **89**, 131 (1993).

[39] C. Bernard et al., "A Lattice Computation of the Decay Constants of B and D Mesons", BNL preprint 49068; C. Bernard et al., Phys. Rev. D **38**, 3540 (1988); G. Martinelli "Heavy Flavour on the Lattice: Results and Prospects", reported at 5th International Symposium on Heavy Flavour Physics, Montreal, 1993; M. B. Gavela et al., Phys. Lett. B **206**, 113 (1988); T. A. DeGrand and R. D. Loft, Phys. Rev. D **38**, 954 (1988).

[40] H. Krasemann, Phys. Lett. B **96**, 397 (1980); M. Suzuki, Phys. Lett. B **162**, 391 (1985); S. Godfrey and N. Isgur, Phys. Rev. D **32**, 189 (1985); S. N. Sinha, Phys. Lett. B **178**, 110 (1986); P. Cea et al., Phys. Lett. B **206**, 691 (1988); S. Capstick and S. Godfrey, Phys. Rev. D **41**, 2856 (1988).

[41] C. Dominguez and N. Paver, Phys. Lett. B **197**, 423 (1987); S. Narison Phys. Lett. B **198**, 104 (1987); L. J. Reinders, Phys. Rev. D **38**, 947 (1988); M. A. Shifman, Usp. Fix. Nauk **151**, 193 (1987) [Sov. Phys. Usp. **30**, 91 (1987)].

[42] R. Ammar et al., (CLEO) Phys. Rev. Lett. **71**, 674 (1993).

[43] B. Barish et al., (CLEO), "First Measuremnt of the Inclusive Rate for the Radiative Penguin Decay $b \to s\gamma$," CONF94-1 (1994).

[44] M. Athanas et al., (CLEO), "A Constraint on $|V_{td}/V_{ts}|$ from $B \to \rho(\omega)\gamma/B \to K^*\gamma$," CONF94-2 (1994).

[45] A. Ali et al., CERN-Th.7118/93 (1993); J. M. Soares, Phys. Rev. D **49**, 283 (1994); S. Narison, Phys. Lett. B **327**, 354 (1994).

[46] Private communication from A. Soni; see also E. Golowich and S. Pakvasa, "Uncertainties from Long Range Effects in $B \to K^*\gamma$," Univ. of Mass. UMHEP-411 (1994).

[47] S. Stone, Mod. Phys. Lett. **A3**, 541, (1988).

[48] D. S. Akerib et al., (CLEO) Phys. Rev. Lett. **67**, 1692 (1991).

[49] M. Gronau, J. Rosner and D. London, Phys. Rev. Lett. **73**, 21 (1994).

[50] M. Gronau and D. Wyler, Phys. Lett. B **265**, 172 (1991); S. Stone, Nucl. Instr. & Meth. **A333**, 15, (1993).